Water Science & Technology

Water Science & Technology Vol 87 No 11, 2597 doi: 10.2166/wst.2023.155

Effects of solvent environment on the spectroscopic properties of tylosin, an experimental and theoretical approach

Aleksandr G. Avramenko and Mindy J. Spiehs*

United States Department of Agriculture, Agricultural Research Service, U.S. Meat Animal Research Center, Livestock Bio-Systems Research Unit, 18d State Spur, Clay Center, NE 68933, USA
*Corresponding author. E-mail: mindy.spiehs@usda.gov

AGA, 0000-0001-5951-0150

ABSTRACT

Tylosin is a commonly used antibiotic in animal medicine. However, it remains unclear how tylosin impacts the broader ecosystem once the host animal has excreted it. One of the main concerns is that it can lead to the development of antibiotic resistance. Therefore, there exists a need to develop systems that remove tylosin from the environment. Utilizing UV irradiation to destroy pathogens is one technique often deployed by scientists and engineers. However, for light-based techniques to be efficient, it is necessary to understand the spectral properties of the material being removed. Steady-state spectroscopy and density functional theory were used to analyze the electronic transitions of tylosin responsible for its strong absorbance in the mid-UV region. It was observed that the absorbance peak of tylosin stems from two transitions in the conjugated region of the molecule. Moreover, these transitions stem from an electronegative region of the molecule, which would allow them to be manipulated by changing solvent polarity. Finally, a polariton model has been proposed, which can be used to initiate the photodegradation of tylosin without the need for direct irradiation of the molecule with UV-B light.

Key words: absorption, DFT (density functional theory), spectroscopy, tylosin, ultraviolet

HIGHLIGHTS

- Tylosin absorption stems from two $\pi-\pi^*$ type transitions of similar energy.
- The pi–pi transitions are located in an electronegative portion of the molecule.
- The FWHM, and thus the lifetime, of the transitions is pH-dependent.
- Absorption of tylosin is quenched in toluene.
- A polariton model is proposed in which 2.97 eV light can be used to initiate tylosin photodegradation.

INTRODUCTION

Antibiotic resistance has emerged as a topic of concern for the scientific community. A particular area of concern is the use of tylosin to maintain livestock health, as up to 80% of the orally administered dosage can be excreted back into the environment by the animal (Stromer *et al.* 2019). Once released into the environment natural processes can transport tylosin through the ecosystem. For example, Dinh *et al.* (2011) detected a concentration of 2.8 ng L^{-1} of tylosin in the Marne River. The authors attributed the presence of tylosin in the river to either the incomplete removal of antibiotics by treatment plants or runoff contamination from nearby agricultural land. Moreover, out of the 23 contaminants tested by the authors, tylosin was one of only three present in the river at a high enough concentration to be detected. Likewise, Kim *et al.* (2012) reported a concentration of tylosin in agricultural soil bordering animal feeding operations at 19.6 μg kg^{-1}. The presence of tylosin in the environment has made it necessary to develop treatment methods that can remove it from the ecosystem. One such method is the usage of light-based technologies.

The use of UV irradiation to sterilize an environment is a well-known concept. When exposed to UV light a molecule can undergo photodegradation, breaking down into simpler molecules, with aromatic compounds especially vulnerable to this decay pathway (Wicks *et al.* 2007). Using light to break down molecules has several advantages. First, since the process uses light as the instrument of degradation, it is easy to use and can be initiated at room temperature. Second, in theory,

light-induced reactions can achieve high rates of conversion as it is easy for irradiated photons to reach most of the sample molecules. Third, light irradiation is most efficient for flat surfaces, such as water. However, this technique has several notable disadvantages, primarily the requirement of specialized UV lamps to achieve optimal results. Indeed, work by Voigt & Jaeger (2017) showed that tylosin could be eliminated via photodegradation in 4 min at pH 3 and pH 7 and 6 min at pH 9 when irradiated by 4.88 eV (254 nm) light at a photon fluence rate of 2 mmol min^{-1} L^{-1}. Therefore, it is possible to efficiently remove antibiotics from water using high-energy UV light. However, UV lamps are energy-intensive, require special safety requirements to operate as many utilize mercury, and require frequent replacement to maintain efficiency (Shin *et al.* 2016). Also, the penetration depth of a photon is inversely proportional to its wavelength; that is, a high-energy, short-wavelength UV photon will not be able to penetrate as deep as a longer, lower energy photon (Saleh & Teich 2007; Wicks *et al.* 2007). Many of the issues of cost and safety concerns could be overcome if sunlight could be harvested as the light source used to degrade antibiotics in wastewater. However, the spectral power density of sunlight falls considerably above 3.1 eV (Pettit 1940). Moreover, the spectrum of sunlight varies with the seasons, with the northern hemisphere exposed to a higher amount of UV irradiation around the summer solstice than the winter solstice (Forsythe & Christison 1930).

While using light to degrade unwanted molecules is a well-established technique, it comes with the caveat that a molecule's UV absorption spectra is dependent on the surrounding environment. A molecule's absorbance may blue shift to a higher energy, red shift to a lower energy, or be heavily suppressed based on the surrounding solvent molecules. In simple terms, a red shift would occur when the solvent molecules act to stabilize the excited state potential energy surface (PES). This may occur if the excited state is more polar than the ground state and is stabilized by a polar solvent (Kelley 2012). The molecule's environment can also influence the lifetime of the excited state. For example, while acting to stabilize the PES of a molecule a solvent can impact the Franck–Condon overlap between the vibrational wavefunctions (Kelley 2012). Because the surrounding molecular environment impacts a molecule's UV spectra, it would, in turn, impact the effectiveness of lamps and photocatalysts used to degrade antibiotics by shifting the absorption spectra of a molecule and reducing the lamp's effectiveness. Therefore, understanding how the spectrum of antibiotic contaminants such as tylosin is impacted under various solvent conditions is imperative in the successful design of effective photodegradation mechanisms.

Porphyrins are one class of molecules that can serve as photocatalysts to initiate the photodegradation of antibiotics, such as tylosin, under lower energy conditions such as sunlight due to the presence of the Soret band, which is a strong absorptive region the molecule possesses in the near UV region. While the spectra of porphyrins have been studied since the 1950s, with the 'Four Orbital' model explaining the behavior of porphyrin spectra, few spectroscopic studies have been conducted on tylosin to analyze its behavior in different solvent conditions (Gouterman 1959). By examining the UV spectra of tylosin, we can approximate its excited state lifetime and infer the molecule's energetic behavior when exposed to different environments. Moreover, it is possible to infer the molecule's structure and PES using computational tools. As a molecule's photoreactivity is determined by how it travels along its PES, understanding it is critical to designing proper photocatalysts (Feist *et al.* 2017).

METHODS

Tylosin A was dissolved in six different solutions to measure its spectral properties. Pharmaceutical standard grade Tylosin was sourced from Sigma-Aldrich and prepared in pH 2.2 deionized (DI) water (15 MΩ) obtained via a Purelab flex purification system to create a 0.0970 mM solution. The acidic DI water was created by titrating 5 mL of acetic acid (Fisher Scientific, 99.5%) with 40 mL DI water. Next, we prepared a neutral DI water solution by dissolving tylosin in a water sample with pH 7.44 at a concentration of 0.0917 mM. A basic solution with pH 11.62 was prepared by titrating 1 mL NaOH (Sigma-Aldrich, 1 N) with 49 mL DI water, and tylosin was added to give a final concentration of 0.0939 mM. A sample of tylosin was then dissolved in toluene to give a final concentration of 0.0982 mM to simulate a non-polar environment. Samples in acetone and acetonitrile were created at a concentration of 0.0917 mM tylosin. Finally, a sample of tylosin was dissolved in 2-propanol to give a final concentration of 0.0939 mM. The toluene was purchased from Sigma-Aldrich, while the acetone, acetonitrile, and 2-propanol was purchased from Fisher Scientific, the solutions were at >99.5% purity. The pH measurements were taken by the Fisher Scientific Orion pH meter.

The steady-state UV–Vis spectra of the created solutions were measured at room temperature (22.5 °C) using a SpectraMax M5 monochromator and a 1 cm cuvette. Density functional theory (DFT) calculations provided in the Gaussian 16 package were used to calculate the molecule's molecular orbitals and vibrational energies. The B3LYP correlation function, along with the 6–31 g(d,p) basis set, was employed for this calculation (Frisch *et al.* 2016). Based on the data obtained from the Gaussian

16 calculations, the observed UV–Vis spectra were modeled to a set of two Gaussian functions using MATLAB software to account for the two transitions that were responsible for the absorbance of the tylosin peak in the UV region. The full width half maximum (FWHM) of the modeled peaks was then extracted from which the lifetime of the excited state was inferred. The Gaussian simulating the lower energy transition is referred to as the first excited state (E_1), while the higher energy transition is dubbed the second excited state (E_2). To compare the vibrational results of the Gaussian calculation, a vibrational spectra of a tylosin powder was obtained using a Nicolet Summit FTIR spectrometer. The Raman data was collected using a Horiba/Jobin Yvon LabRAM HR800 Raman Microscope employing a 633 nm laser source, two averages of 30 s were used to acquire the data. Lastly, a MATLAB model of a polariton was constructed using the wave transfer matrix method of approximating optical spectra, describing how a polariton can be used to degrade a photoactive molecule such as tylosin.

RESULTS

Figure 1 reports the spectra of tylosin under different solvent environments. The DFT calculation showed that two transitions are responsible for the peak centered around 4.30 eV shown in Figure 1. A first excited state (E_1) HOMO-2 to LUMO + 1 transition with an oscillator strength of 0.67931, and a second excited state (E_2) HOMO-3 to a LUMO transition with an oscillator strength of 0.57029. The orbitals involved in these transitions are shown in Figure 2. The DFT calculation also predicts an energy transition with an oscillator strength of 0.66385 at 5.40 eV stemming from a HOMO-2 to a LUMO transition. However, this transition was likely blue shifted outside the observable bounds of the instrument. The UV spectra of the peak at 4.30 eV were modeled using two Gaussian functions to simulate the two near degenerate transitions responsible for its appearance. The FWHM of the two Gaussian peaks is listed in Table 1, the detailed description of the fits can be found in the Supplementary material. A slight increase in the FWHM of the E_2 ($p = 0.0006210$) was observed with an increase in pH. An opposite phenomenon is observed with the FWHM of E_1. The FWHM of E_1 is on average 70.54% smaller than that of E_2 in all solvents except toluene. For the tylosin sample dissolved in toluene, the FWHM of E_2 was 53.65% smaller than E_1. The attenuation coefficient of the transition was empirically extracted using the well-established relationship between the peak absorbance and concentration described by the Beer–Lambert law, which is reported in Table 1.

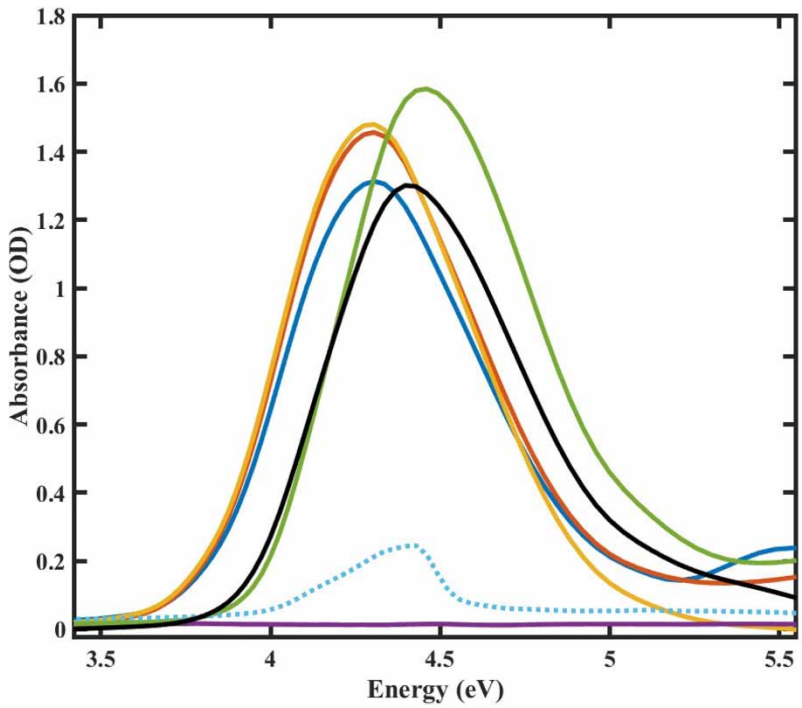

Figure 1 | UV–Vis spectra of tylosin in different solvent environments. These included water at pH 2.2 (blue), pH 7.44 (red) pH 11.62 (yellow), acetone (purple), acetonitrile (green), toluene (dashed cyan), and 2-propanol (black). No detectable peak was observed when tylosin was dissolved in acetone (purple). Please refer to the online version of this paper to see this figure in colour: https://dx.doi.org/10.2166/wst.2023.155.

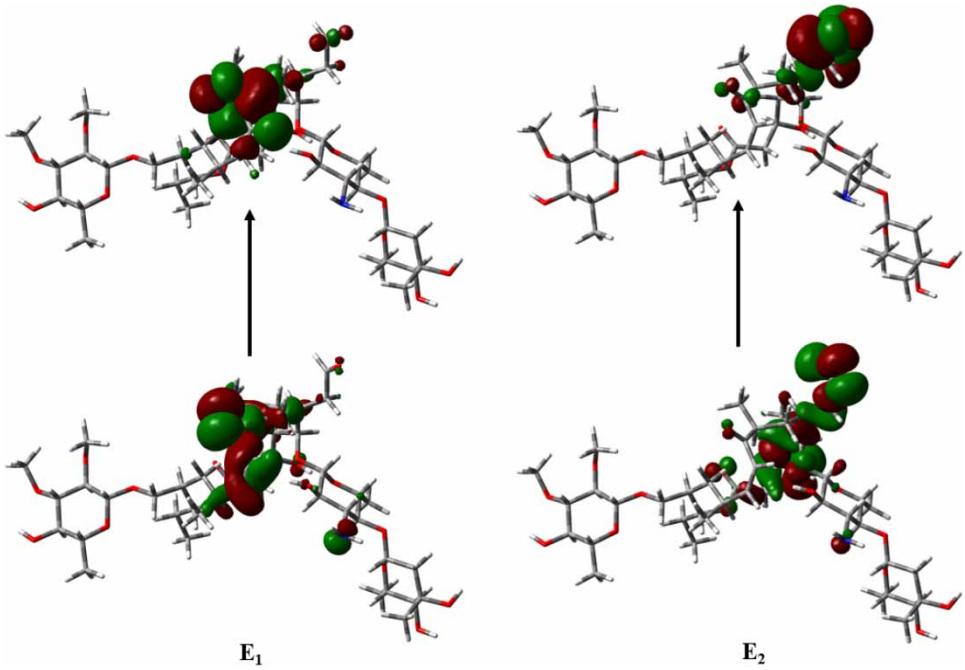

Figure 2 | Molecular orbitals of tylosin involved in the transition that is responsible for the molecule's strong absorbance in the UV region.

Table 1 | The calculated FWHM of the two states that convolve to produce the tylosin peak near 4.30 eV

Solvent	FWHM (eV) (E_1)	FWHM (eV) (E_2)	Observed peak max (eV)	α ($M^{-1}cm^{-1}$)
DI water (pH 2.2)	0.2761	0.3681	4.306	13,853
DI water (pH 7.44)	0.2819	0.3760	4.306	16,255
DI water (pH 11.62)	0.2552	0.4015	4.306	15,761
Water *p*-value (FWHM)		0.0006210		
Toluene	0.2382	0.1104	4.397	2327
Acetone	NA	NA	NA	NA
Acetonitrile	0.2966	0.4012	4.460	17,279
2-propanol	0.3265	0.4891	4.397	13,855

The peak max and attenuation coefficient were calculated from the observed spectra. No spectra in the UV region were observed when tylosin was dissolved in acetone. The *p*-value comparing the FWHM of the two transitions in water is also provided.

The molecular orbitals responsible for the strong transition in the UV region are shown in Figure 2. As predicted by previous authors, the strong tylosin absorbance stems from the presence of conjugated double bonds (Voigt & Jaeger 2017). An electrostatic potential surface (ESP) for the molecule is presented in Figure 4, demonstrating that the conjugated region of the molecule responsible for the UV absorbance is more electronegative than the rest of the molecule.

DISCUSSION

Observations of the FWHM of tylosin in the UV region revealed that the FWHM of E_1 decreased as the pH of DI water increased, with the opposite phenomenon occurring in E_2. A decrease in FWHM suggests an increase in the lifetime of the excited state (Saleh & Teich 2007). Therefore, the increased H^+ concentration at lower pH act to stabilize the E_2 energy level. On the contrary, a decrease in the H^+ concentration at higher pH seems to stabilize the E_1 energy level, as seen in Figure 3. The results suggest that the high polarity of acetonitrile stabilizes the excited state in comparison to

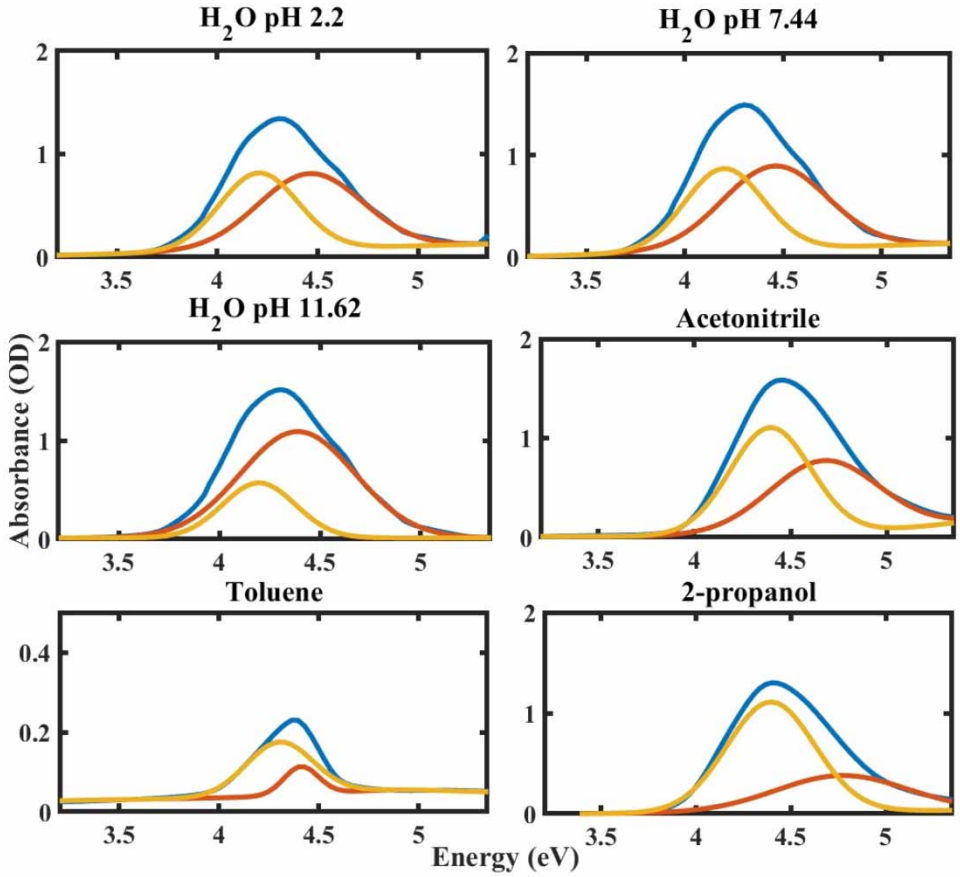

Figure 3 | The absorbance peak of tylosin (blue) in various solvents plotted versus the constituent E_1 (yellow) and E_2 (red) peaks as predicted by Gaussian calculations that comprise the observed peak. Please refer to the online version of this paper to see this figure in colour: https://dx.doi.org/10.2166/wst.2023.155.

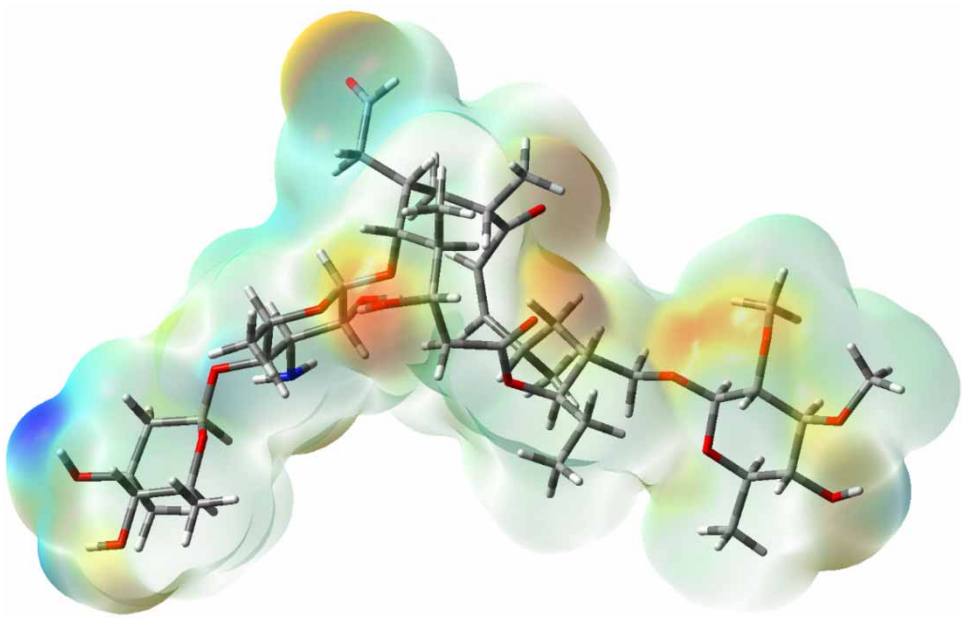

Figure 4 | Calculated electrostatic potential map of tylosin. The red color denotes a negative charge while a blue color denotes a positive charge. Please refer to the online version of this paper to see this figure in colour: https://dx.doi.org/10.2166/wst.2023.155.

2-propanol. However, it seems that steric hindrance must also play a role since the FWHM of both excited states were calculated to be higher when tylosin was dissolved in 2-propanol as compared to water. When dissolved in the non-polar solvent toluene, the lifetimes of the excited states become inverted, with the FWHM of the second excited state calculated to be smaller than that of the first excited state.

When the molecule was dissolved in toluene, a drastic decrease in the attenuation coefficient was observed, as seen in Table 1. Several factors might contribute to such an outcome. First, toluene possesses its own conjugate bond system and absorbs strongly in the same UV region as tylosin (Ginsburg *et al.* 1946). Therefore, it may have effectively photobleached the system, outcompeting the tylosin for the available photons. Second, because tylosin absorbs in the same UV region, the excited state PES of the two molecules can form conical intersections, allowing for the excited tylosin to quickly disperse energy into the PES of the toluene (Kelley 2012).

It is also noted that while the maximum peak energy of tylosin does not shift in most solvents, there is a considerable blue shift of 154 meV when tylosin is dissolved in acetonitrile, accompanied by an increase in the attenuation coefficient. A blue shift indicates an increase in the energy gap between the ground and excited states, implying that the ground state of tylosin is more polar than the excited state (Reichardt 1994). The polar acetonitrile molecules interact with the electronegative conjugated region of tylosin to stabilize the molecule, allowing the ground state to relax into a lower energy state. Tylosin molecules would require slightly larger light energy to reach the excited states in a more relaxed configuration. However, for a molecular electron transition to occur, there must be some overlap between the ground and excited state wave functions. As seen in Table 1, this phenomenon is also observed to as smaller degree in 2-propanol, in which the peak is shifted by 91 meV. 2-Propanol possesses a polarity intermediate of water and acetonitrile, which likely explains why the tylosin dissolved in propanol has an absorption maximum intermediate between the two solvents (Kosower 1957).

The probability of making a transition between states depends on the complex conjugate of the transition dipole moment $\mu_{ab} = \psi_b|r|\psi_a$, where r is the dipole operator, which is a vector dependent on the position and charge of electrons and nuclei within the molecule (Gieseking *et al.* 2014). Meanwhile, ψ_a and ψ_b are the two wavefunctions describing the eigenstates of the molecule involved in the transition. Because eigenstates are typically described in Hilbert (vector) space if ψ_a and ψ_b are orthogonal to each other, there will be no transition (Mukamel 1995). For this reason, a molecule stabilized within its ground state configuration can have a better overlap with the excited state orbitals, resulting in a larger attenuation coefficient.

The IR and Raman spectra of tylosin were calculated by applying DFT via Gaussian software, as seen in Figures 5 and 7. Based on the calculations, the most vibrationally active modes of tylosin lie in the carbon–oxygen double bond region of the spectra, which is in line with previously conducted studies into the Fourier-transformed infrared (FTIR) spectra of tylosin (Freitas *et al.* 2020). On the contrary, much of the molecule's Raman activity falls around the higher energy C–H region. Compared to experimental vibrational IR spectra in Figure 6, the calculated spectra is blue shifted by approximately 100 cm^{-1}. Moreover, the experimental data shows a broad 3,500 cm^{-1} OH stretch area, as opposed to several distinct peaks seen in the calculated IR spectrum. These discrepancies are likely due to the calculation being performed under 'single molecule' and vacuum assumptions, while experimental measurements are carried out in a bulk tylosin powder. Figures 7 and 8 display

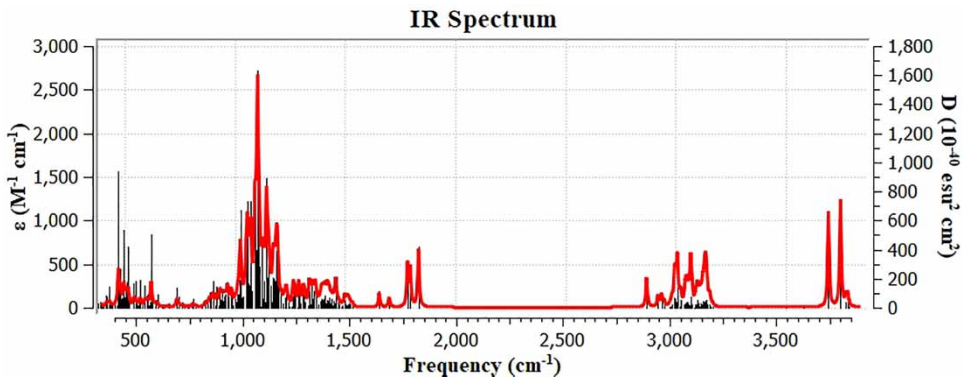

Figure 5 | Calculated IR spectra of tylosin.

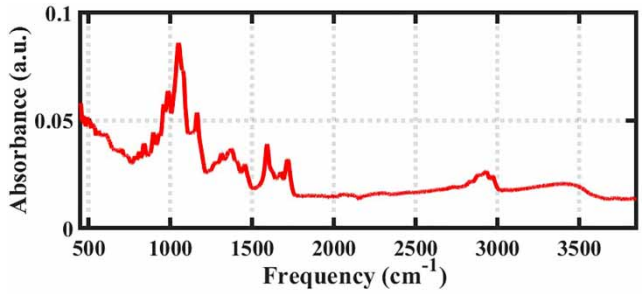

Figure 6 | Experimentally measured IR spectra of tylosin.

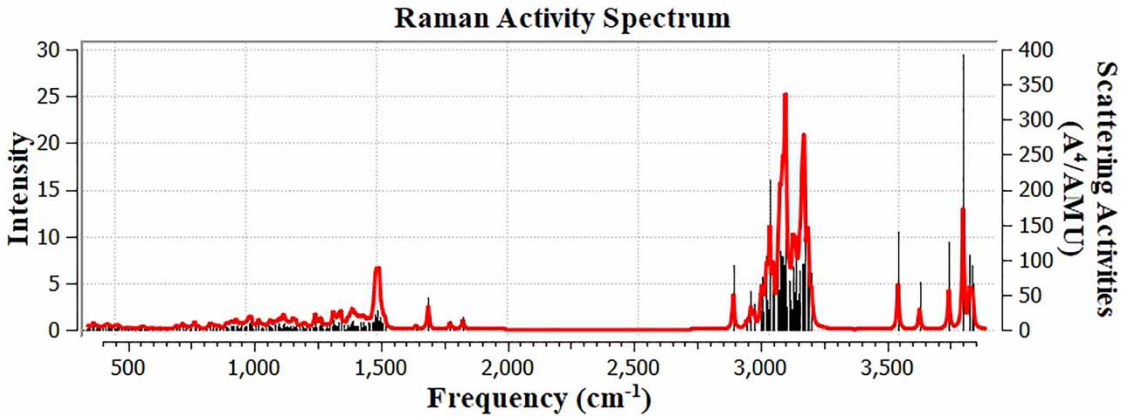

Figure 7 | Calculated Raman spectra of tylosin.

the calculated and measured Raman spectra of tylosin. Note the simultaneous red shift in the C–H region, along with a blue shift in the C–C double bond region in the experimental data as compared to the calculated. While this is most likely an artifact of the background correction to subtract any fluorescence induced by the Raman laser, the possibility that the PES of the molecule is impacted by intermolecular forces cannot be discounted. The vibrational modes of a molecule provide valuable information which can be used to estimate the PES of a molecule (Laane 1987). Simply put, it is possible to use a harmonic oscillator model to estimate the potential energy based on the vibrational spectra.

Lastly, we propose a theoretical model in which a porphyrin-based cavity polaritons can be used as a tool to degrade tylosin. Voigt & Jaeger (2017) demonstrated that tylosin quickly degrades when exposed to high-energy UV radiation. Several issues of using high-energy UV light for such purposes are discussed in the introduction, such as safety concerns and its short penetration depth. However, it may be possible to use lower energy light to form cavity polaritons, which will then initiate the

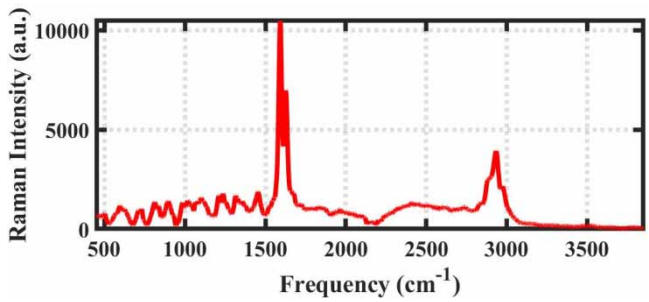

Figure 8 | Experimentally measured Raman spectra of tylosin.

decay of the tylosin molecule. Cavity polaritons are formed when a molecule is placed inside an optical cavity whose photon is tuned to the excitation wavelength of the molecule. If the molecule and the photon exchange energy faster than the decay of either state, they form a polariton state, a quasi-particle with hybrid characteristics of both light and matter. Two polariton states will form when this process occurs, a lower and an upper polariton (Ebbesen 2016). As indicated by its name, the upper polariton energy will be higher than that of the molecule in free space.

When the molecule forms a polariton state, it will have a partially photonic, or 'light-like' characteristic, with the energy of the polariton states being defined as:

$$E_{\mathrm{LP/UP}}(\theta) = \frac{E_{\mathrm{ph}(\theta)} + E_{\mathrm{ex}}}{2} \pm \frac{1}{2}\sqrt{(E_{\mathrm{ph}(\theta)} - E_{\mathrm{ex}})^2 + V^2}$$

where $E_{\mathrm{LP/UP}}$ are the two polariton states being formed by the interaction of the photon with the porphyrin, E_{ph} is the energy of the photon, E_{ex} is the excitation energy of the porphyrin, and V is the coupling strength between the photon and molecular excitation (Avramenko & Rury 2021). This formula demonstrates that the energy of polaritons is a convolution of the photonic and excitonic states that form them. Moreover, the 'light-like' nature of the polariton states will depend on the sample angle (θ) as the polariton state is dispersive. Therefore, it may be feasible to initiate polariton formation at lower light energies with a molecule such as tetraphenylporphyrin, which will then create an upper polariton at a higher energy that can initiate the photodegradation of tylosin. The formation of polaritons by embedding porphyrin molecules into nano-scale cavities has been well established (Avramenko & Rury 2021). Moreover, this process has been shown to impact the photophysics of the molecule by altering the innate rate of internal conversion within the porphyrin molecule (Galego *et al.* 2016; Avramenko & Rury 2020). By using the wave transfer matrix method as described by Saleh & Teich (2007), it is possible to construct simulated spectra of a polariton formed as a result of a tetraphenylporphyrin strongly coupling to a 2.97 eV (417 nm) photon of a cavity mode. The index of refraction of the optical media used to create the cavity was estimated using the Sellmeier equations (Malitson 1965; Kim & Sarangan 2007; Blümel *et al.* 2016). The details of the simulations can be found in the Supplementary material. As seen in Figure 9, there is an overlapping area between the spectrum of the upper branch of the cavity polariton and that of the tylosin excitation. Because of the polariton's light-like nature, this overlap could be used to break down the tylosin molecule while only trapping 2.97 eV (417 nm) light inside the cavity, as opposed to the 4.88 eV (254 nm) light used by Voigt & Jaeger (2017).

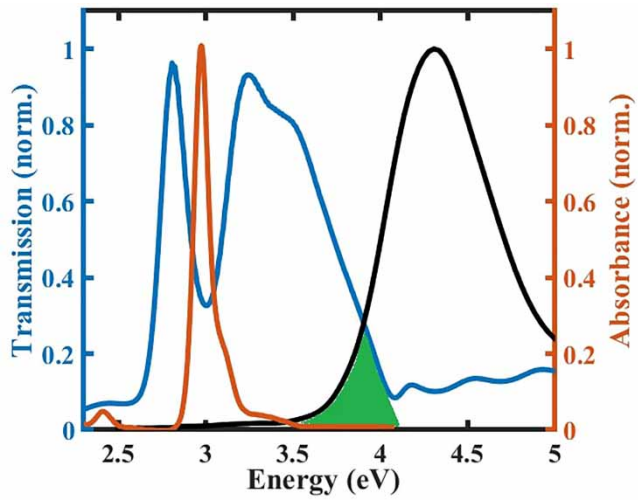

Figure 9 | Calculated spectrum of a polariton showing an overlap (green) between the upper polariton branch transmittance (blue) and that of the tylosin (black) absorbance. The absorption spectra of the porphyrin molecule is presented in red for reference. Please refer to the online version of this paper to see this figure in colour: https://dx.doi.org/10.2166/wst.2023.155.

CONCLUSIONS

In this study, steady-state spectroscopy and computational tools were used to analyze the spectra of tylosin under different solvent conditions, concluding that the UV peak in tylosin is a result of two $\pi-\pi^*$ type transitions of similar intensity. The orbitals involved in these transitions are centered around an electronegative portion of the molecule, making them particularly sensitive to solvent polarization effects. The spectroscopic activity of the molecule was also greatly reduced when dissolved in a solvent that is also optically active in the same region as itself, such as toluene. Finally, an optical model of a porphyrin polariton was constructed, which indicates that the partially photon-like nature of the upper branch of the upper polariton may be able to initiate the photodegradation of tylosin. This fundamental information can further advance light-based techniques to break down tylosin.

ACKNOWLEDGEMENTS

The spectral measurements were performed at the U.S. Meat Animal Research Center, Animal Health Genomics Research Unit in Clay Center, NE. Density functional theory calculations were performed using Wayne State University's High-Performance Computing system. The vibrational measurements were carried out with the help of the University of Nebraska-Kearney's Department of Chemistry. Mention of a trade name, proprietary product, or specific agreement does not constitute a guarantee or warranty by the USDA and does not imply approval of the inclusion of other products that may be suitable. USDA is an equal opportunity provider and employer.

DATA AVAILABILITY STATEMENT

All relevant data are included in the paper or its Supplementary Information.

CONFLICT OF INTEREST

The authors declare there is no conflict.

REFERENCES

Avramenko, A. G. & Rury, A. S. 2020 Quantum control of ultrafast internal conversion using nanoconfined virtual photons. *The Journal of Physical Chemistry Letters* **11** (3), 1013–1021. https://doi:10.1021/acs.jpclett.9b03447.

Avramenko, A. G. & Rury, A. S. 2021 Local molecular probes of ultrafast relaxation channels in strongly coupled metalloporphyrin-cavity systems. *The Journal of Chemical Physics* **155** (6), 064702. https://doi:10.1063/5.0055296.

Blümel, R., Bağcioğlu, M., Lukacs, R. & Kohler, A. 2016 Infrared refractive index dispersion of polymethyl methacrylate spheres from Mie ripples in Fourier-transform infrared microscopy extinction spectra. *Journal of the Optical Society of America A* **33**, 1687–1696. https://doi:10.1364/JOSAA.33.001687.

Dinh, T., Quoc, F. A., Moreau-Guigon, E., Eurin, J., Chevreuil, M. & Labadie, P. 2011 Measurement of trace levels of antibiotics in river water using on-line enrichment and triple-quadrupole LC–MS/MS. *Talanta* **85**, 1238–1245. https://doi.org/10.1016/j.talanta.2011.05.013.

Ebbesen, T. W. 2016 Hybrid light–matter states in a molecular and material science perspective. *Accounts of Chemical Research* **49** (11), 2403–2412. https://doi:10.1021/acs.accounts.6b00295.

Feist, J., Galego, J. & Garcia-Vidal, F. J. 2017 Polaritonic chemistry with organic molecules. *ACS Photonics* **5** (1), 205–216. https://doi:10.1021/acsphotonics.7b00680.

Forsythe, W. E. & Christison, F. 1930 Ultraviolet radiation from the sun and heated tungsten. *Journal of the Optical Society of America* **20** (7), 396. https://doi:10.1364/JOSA.20.000396.

Freitas, A. G., Magalhães, B. E., Minho, L. A., Leão, D. J., Santos, L. S. & Fernandes, S. 2020 FTIR spectroscopy with chemometrics for determination of tylosin residues in milk. *Journal of the Science of Food and Agriculture* **101** (5), 1854–1860. https://doi:10.1002/jsfa.10799.

Frisch, M. J., Trucks, G. W., Schlegel, H. B., Scuseria, G. E., Robb, M. A., Cheeseman, J. R., Scalmani, G., Barone, V., Petersson, G. A., Nakatsuji, H., Li, X., Caricato, M., Marenich, A. V., Bloino, J., Janesko, B. G., Gomperts, R., Mennucci, B., Hratchian, H. P., Ortiz, J. V., Izmaylov, A. F., Sonnenberg, J. L., Williams-Young, D., Ding, F., Lipparini, F., Egidi, F., Goings, J., Peng, B., Petrone, A., Henderson, T., Ranasinghe, D., Zakrzewski, V. G., Gao, J., Rega, N., Zheng, G., Liang, W., Hada, M., Ehara, M., Toyota, K., Fukuda, R., Hasegawa, J., Ishida, M., Nakajima, T., Honda, Y., Kitao, O., Nakai, H., Vreven, T., Throssell, K., Montgomery, J. A., Peralta, J. E. & Ogliaro, F., Bearpark, M. J., Heyd, J. J., Brothers, E. N., Kudin, K. N., Staroverov, V. N., Keith, T. A., Kobayashi, R., Normand, J., Raghavachari, K., Rendell, A. P., Burant, J. C., Iyengar, S. S., Tomasi, J., Cossi, M., Millam, J. M., Klene, M., Adamo, C., Cammi, R., Ochterski, J. W., Martin, R. L., Morokuma, K., Farkas, O., Foresman, J. B. & Fox, D. J. 2016 *Gaussian 16*. Gaussian, Inc., Wallingford, CT.

Galego, J., Garcia-Vidal, F. J. & Feist, J. 2016 Suppressing photochemical reactions with quantized light fields. *Nature Communications* **7**, 13841. https://doi:10.1038/ncomms13841.

Gieseking, R. L., Mukhopadhyay, S., Risko, C. & Brédas, J. L. 2014 Impact of the nature of the excited-state transition dipole moments on the third-order nonlinear optical response of polymethine dyes for all-optical switching applications. *ACS Photonics* **1** (3), 261–269. https://doi:10.1021/ph4001444.

Ginsburg, N., Robertson, W. W. & Matsen, F. A. 1946 The near ultraviolet absorption spectrum of toluene vapor. *The Journal of Chemical Physics* **14** (9), 511–517. https://doi:10.1063/1.1724185.

Gouterman, M. 1959 Study of the effects of substitution on the absorption spectra of porphin. *The Journal of Chemical Physics* **30** (5), 1139–1161. https://doi:10.1063/1.1730148.

Kelley, A. M. 2012 *Condensed-Phase Molecular Spectroscopy and Photophysics Kelley/Condensed-Phase Molecular Spectroscopy and Photophysics*. John Wiley & Sons, Inc, Hoboken, NJ, USA.

Kim, J. P. & Sarangan, A. M. 2007 Temperature-dependent Sellmeier equation for the refractive index of $Al_xGa_{1-x}As$. *Optics Letters* **32** (5), 536. https://doi:10.1364/ol.32.000536.

Kim, S.-C., Chung, D. Y., Kim, K. H., Lee, J. H., Kim, H. K., Yang, J. E., Ok, Y. S. & Almarwei, Y. A. O. 2012 Concentration and environmental loading of veterinary antibiotics in agricultural irrigation ditches. *Korean Journal of Soil Science and Fertilizer* **45** (6), 867–876. https://doi:10.7745/kjssf.2012.45.6.867.

Kosower, E. M. 1957 The effect of solvent on spectra. I. A new empirical measure of solvent polarity: Z-values. *Journal of the American Chemical Society* **80** (13), 3253–3260. https://doi.org/10.1021/ja01546a020.

Laane, J. 1987 Determination of vibrational potential energy surfaces from Raman and infrared spectra. *Pure and Applied Chemistry* **59** (10), 1307–1326. https://doi:10.1351/pac198759101307.

Malitson, I. H. 1965 Interspecimen comparison of the refractive index of fused silica. *Journal of the Optical Society of America* **55** (10), 1205. https://doi:10.1364/josa.55.001205.

Mukamel, S. 1995 *Principles of Nonlinear Optical Spectroscopy*. Oxford University Press, New York; Oxford.

Pettit, E. 1940 Spectral energy-curve of the sun in the ultraviolet. *The Astrophysical Journal* **91**, 159. https://doi:10.1086/144155.

Reichardt, C. 1994 Solvatochromic dyes as solvent polarity indicators. *Chemical Reviews* **94** (8), 2319–2358. https://doi:10.1021/cr00032a005.

Saleh, B. & Teich, M. 2007 *Fundamentals of Photonics*, 2nd edn. John Wiley & Sons, Inc, New York.

Shin, J. Y., Kim, S. J., Kim, D. K. & Kang, D. H. 2016 Fundamental characteristics of deep-UV light-emitting diodes and their application to control foodborne pathogens. *Applied and Environmental Microbiology* **82** (1), 2–10. https://doi:10.1128/aem.01186-15.

Stromer, B. S., Woodbury, B. & Williams, C. F. 2019 The efficacy of three diatomaceous earth sources for removing tylosin from aqueous systems. *Journal of Environmental Quality* **48** (6), 1863–1871. https://doi:10.2134/jeq2018.11.0409.

Voigt, M. & Jaeger, M. 2017 On the photodegradation of azithromycin, erythromycin and tylosin and their transformation products – a kinetic study. *Sustainable Chemistry and Pharmacy* **5**, 131–140. https://doi:10.1016/j.scp.2016.12.001.

Wicks, Z. W., Jones, F. N., Pappas, S. P. & Wicks, D. A. 2007 *Organic Coatings*. John Wiley & Sons, Inc, Hoboken, NJ, USA. https://doi:10.1002/047007907x.

First received 21 October 2022; accepted in revised form 8 May 2023. Available online 19 May 2023